Computational Materials Science 121 (2016) 97–105

Contents lists available at ScienceDirect

Computational Materials Science

journal homepage: www.elsevier.com/locate/commatsci

Phonon spectral energy density analysis of solids: The **k** point reduction in the first Brillouin zone of FCC crystals and a case study on solid argon

Zuyuan Wang, Xiulin Ruan *

School of Mechanical Engineering and the Birck Nanotechnology Center, Purdue University, West Lafayette, IN 47907, USA

ARTICLE INFO

Article history:
Received 30 November 2015
Received in revised form 8 March 2016
Accepted 8 April 2016
Available online 11 May 2016

Keywords:
FCC crystals
First Brillouin zone
Thermal conductivity
Molecular dynamics
Phonon transport
Solid argon

ABSTRACT

Many crystals of scientific and technical importance have the face-centered cubic (FCC) lattice. Computational studies of electronic, thermal, and optical properties of FCC crystals usually involve the first Brillouin zone. In this work, we examine the geometry and discretization of the first Brillouin zone of FCC crystals. We report the coordinates of the high symmetry **k** points in the first Brillouin zone and a systematic way of determining the coordinates of the symmetry **k** points. We find that using the symmetry **k** points could reduce the total number of **k** points by as much as 97.92% and thus greatly reduce the computational cost. We propose a formula for calculating lattice thermal conductivity by using phonon properties at the symmetry **k** points. The formula is validated by calculating the thermal conductivity of solid argon in the temperature range from 10 to 80 K with the phonon spectral energy density (SED) method and comparing the results with those from equilibrium molecular dynamics (EMD) simulations and experiments.

1. Introduction

Face-centered cubic (FCC) lattice is a type of cubic lattice consisting of lattice sites at the corners and face centers. Because of the large packing fraction (0.740) and the associated low cohesive energy [1], FCC lattice is adopted as the lattice by many crystalline materials, such as the solid phase of noble gases (*e.g.*, helium, neon, argon, and krypton) and many metals (*e.g.*, aluminum, copper, silver, gold, and lead). If we consider the lattice of materials of the diamond structure [1], which is seen in crystals like diamond, silicon, and germanium, as two interpenetrating FCC lattices with one translated with respect to the other along a body diagonal by a distance of 1/4 of the body diagonal length, then the lattice could be treated as an FCC lattice with two identical basis atoms at each lattice site. Similarly, the lattice of materials of the cubic zinc sulfide structure [1], which exists in crystals like ZnS, SiC, GaAs, InAs, and InP, have an FCC lattice with two different basis atoms at each lattice site. Because of the scientific and technical importance of the materials formed from FCC lattices, they appear frequently in research, in which their many properties (*e.g.*, electronic [1–5], thermal [1,6–9], and optical [10–13]) are investigated. In studies involving analysis in the frequency domain (or the reciprocal space), it is inevitable to examine the first Brillouin zone. To facilitate such analysis, it is essential to have a good knowledge of the first Brillouin zone of FCC crystals.

In computational studies, the first Brillouin zone is usually sampled with a set of discrete **k** points as a result of the finite size of the simulated material system. Similar to an **R** point, which represents a point in the direct space, a **k** point represents a point in the reciprocal space. It is known that $\mathbf{R} = n_1\mathbf{a}_1 + n_2\mathbf{a}_2 + n_3\mathbf{a}_3$ and $\mathbf{k} = \lambda_1\mathbf{b}_1 + \lambda_2\mathbf{b}_2 + \lambda_3\mathbf{b}_3$, where $(\mathbf{a}_1, \mathbf{a}_2, \mathbf{a}_3)$ is a set of basis vectors in the direct space, (n_1, n_2, n_3) are the coordinates of the **R** point, $(\mathbf{b}_1, \mathbf{b}_2, \mathbf{b}_3)$ is a set of basis vectors in the reciprocal space, and $(\lambda_1, \lambda_2, \lambda_3)$ are the coordinates of the **k** point. For numerical analysis in the reciprocal space, a denser **k** point grid (or more **k** points) means a higher computational cost. Therefore, it is desired to reduce the number of **k** points, particularly for first-principles calculations. Previously, researchers have considered the first Brillouin zone using different approaches, such as resolving the entire first Brillouin zone, considering the irreducible first Brillouin zone, and focusing on high symmetry directions by assuming the first Brillouin zone to be spherical and the properties to be isotropic. The accuracy and computational cost of the three approaches both decreases in the order. Because of the moderate computational cost and the good accuracy associated with the second approach, it is widely used in the relevant spectral analysis in the reciprocal space [14,15].

Solid argon is an FCC crystal with a lattice constant of 5.30 Å at 0 K [16]. The interatomic interactions are commonly assumed to be

* Corresponding author.
E-mail address: ruan@purdue.edu (X. Ruan).

http://dx.doi.org/10.1016/j.commatsci.2016.04.018
0927-0256/

pure van der Waals forces and characterized with the Lennard-Jones potential [17]. Because of the relatively simple crystal structure and interatomic potential, solid argon has been widely used as a benchmark material for many novel numerical methods of calculating lattice thermal conductivities and phonon properties, such as the equilibrium molecular dynamics (EMD) simulations with the Green–Kubo method [18–20], the nonequilibrium molecular dynamics (NEMD) simulations [21], the anharmonic lattice dynamics (ALD) method [22,23], the normal mode analysis (NMA) method [24–26], and the spectral energy density (SED) analysis method [24,25,27,28].

In this work, we examine the geometry and discretization of the first Brillouin zone of FCC crystals. We report a way of reducing the number of **k** points by considering the symmetry of the first Brillouin zone and determine the variation of the number of symmetry **k** points with the **k** point grid size. We also propose a formula for calculating lattice thermal conductivities based on phonon properties at the symmetry **k** points. To validate the formula, we calculate the thermal conductivity of solid argon in the temperature range from 10 to 80 K using the SED method and compare the results with those from EMD simulations and experiments. In addition, we show results on the phonon relaxation times in solid argon and the thermal conductivity accumulation with the phonon wavelength and mean free path (MFP).

2. Geometry considerations

The first Brillouin zone is essential for the analysis of the electronic, thermal, and optical properties of crystals. In this section, we examine the geometrical features of the first Brillouin zone of FCC crystals.

Fig. 1(a) shows a conventional unit cell of an FCC lattice with a lattice constant a. Fig. 1(b) shows the first Brillouin zone of the FCC lattice which has a lattice constant of $\frac{4\pi}{a}$. It is seen that the first Brillouin zone has 14 faces, including six squares and eight hexagons. The six squares can be represented by the following equations: $|k_x| = \frac{2\pi}{a}$, $|k_y| = \frac{2\pi}{a}$, and $|k_z| = \frac{2\pi}{a}$; the eight hexagons can be represented by the following equation: $|k_x| + |k_y| + |k_z| = \frac{3}{2}\frac{2\pi}{a}$. In terms of the reduced coordinates $\left(k_x^*, k_y^*, k_z^*\right)$, which are $\frac{2\pi}{a}(k_x, k_y, k_z)$, the equations become $|k_x^*| = 1$, $\left|k_y^*\right| = 1$, and $|k_z^*| = 1$ for the squares and $|k_x^*| + \left|k_y^*\right| + |k_z^*| = \frac{3}{2}$ for the hexagons.

Because of the geometrical symmetry of the first Brillouin zone, it is invariant under many symmetry operations (*e.g.*, rotation, reflection, inversion). Fig. 1(b) shows the high symmetry points, including the Γ, K, L, U, W, and X points. Fig. 1(c) shows a high symmetry point X^*, which is an X point belonging to a neighboring first Brillouin zone and is usually used in calculations of phonon dispersions and electronic band structures.

In Fig. 1(d), we show the coordinates of the high symmetry **k** points in the first Brillouin zone (see Fig. 1(b) and (c)) with respect to the basis vector sets $(\hat{\mathbf{x}}, \hat{\mathbf{y}}, \hat{\mathbf{z}})$ and $(\mathbf{b}_1, \mathbf{b}_2, \mathbf{b}_3)$, respectively. In many computational packages (*e.g.*, GULP [29], ABINIT [30,31], QUANTUM-EXPRESSO [32], and VASP [33–35]), it is the coordinates with respect to the latter basis vector set that are used. It is worth mentioning that using the X^* point instead of the X point results in smoother phonon dispersion and electronic band structure curves along the high symmetry direction Γ–K–X in the relevant calculations.

3. Symmetry considerations

It is well known that the number of degrees of freedom is independent of the choice of the coordinate system. The number of

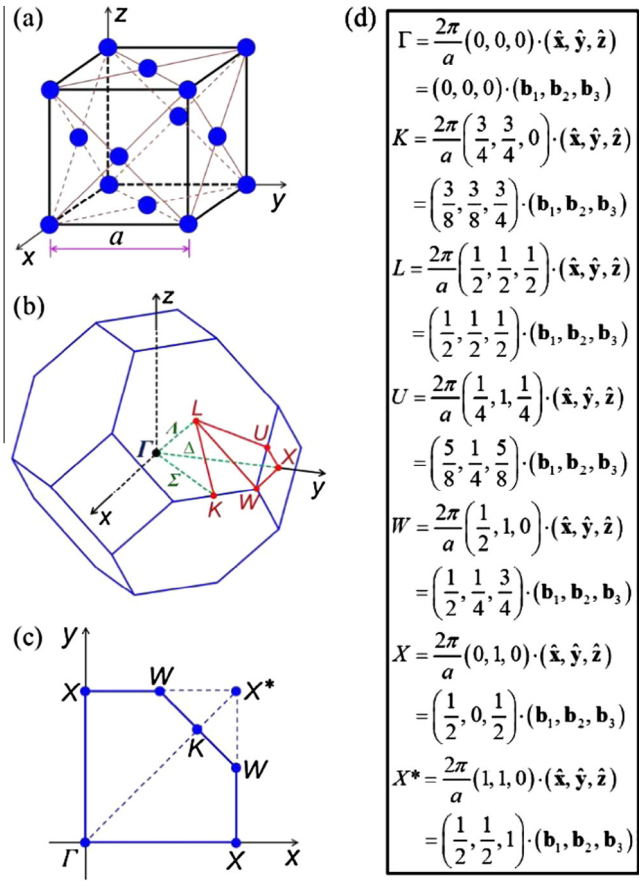

Fig. 1. (a) A conventional unit cell of an FCC lattice with a lattice constant a. (b) The first Brillouin zone of an FCC lattice, including the high symmetry **k** points and directions. (c) A schematic showing X^*, which is an X point in a neighboring first Brillouin zone. (d) The coordinates of the high symmetry **k** points with respect to basis vector sets $(\hat{\mathbf{x}}, \hat{\mathbf{y}}, \hat{\mathbf{z}})$ and $(\mathbf{b}_1, \mathbf{b}_2, \mathbf{b}_3)$, respectively.

degrees of freedom must be the same no matter a material system is analyzed in the direct or reciprocal space. For a cubic FCC crystal with N_{cell} unit cells (usually conventional unit cells) along each of the $\hat{\mathbf{x}}$, $\hat{\mathbf{y}}$, and $\hat{\mathbf{z}}$ directions, the total number of degrees of freedom is $3N_{\text{cell}}^3 N_{\text{site}} N_{\text{basis}}$, where the leading "3" indicates the three directions ($\hat{\mathbf{x}}$, $\hat{\mathbf{y}}$, and $\hat{\mathbf{z}}$), N_{site} represents the number of lattice sites in each unit cell, which is four for FCC lattices, and N_{basis} is the number of basis atoms at each lattice site. In the corresponding reciprocal space, the number of degrees of freedom is $3N_{\text{basis}}N_{\mathbf{k},\text{total}}$, where $N_{\mathbf{k},\text{total}}$ is the total number **k** points in the first Brillouin zone. For FCC crystals, it must hold that $3N_{\text{basis}}N_{\mathbf{k},\text{total}} = 12N_{\text{cell}}^3 N_{\text{basis}}$, which gives $N_{\mathbf{k},\text{total}} = 4N_{\text{cell}}^3$. Since $N_{\mathbf{k},\text{total}}$ is proportional to N_{cell}^3, it increases quickly as N_{cell} increases. Therefore, it is of great importance that the number of distinct **k** points (and thus the associated computational cost) could be reduced.

Considering the symmetry of the first Brillouin zone provides an effective way of reducing the number of **k** points that need to be directly resolved. In Fig. 2, we show the first Brillouin zone of an FCC crystal with $6 \times 6 \times 6$ conventional unit cells. While the **k** points corresponding to an infinitely large crystal could approximately be considered continuous, the **k** points for crystals of finite sizes are discrete. According to the analysis above, there are in total 4×6^3 (=864) **k** points in the first Brillouin zone. We break down the **k** points into layers according to the k_z^* values, which are the z coordinates of the **k** points [with respect to $(\hat{\mathbf{x}}, \hat{\mathbf{y}}, \hat{\mathbf{z}})$ and normalized by $\frac{2\pi}{a}$]. Alternatively, the **k** points could be classified into corner, edge, surface, and interior **k** points. In this classification, the

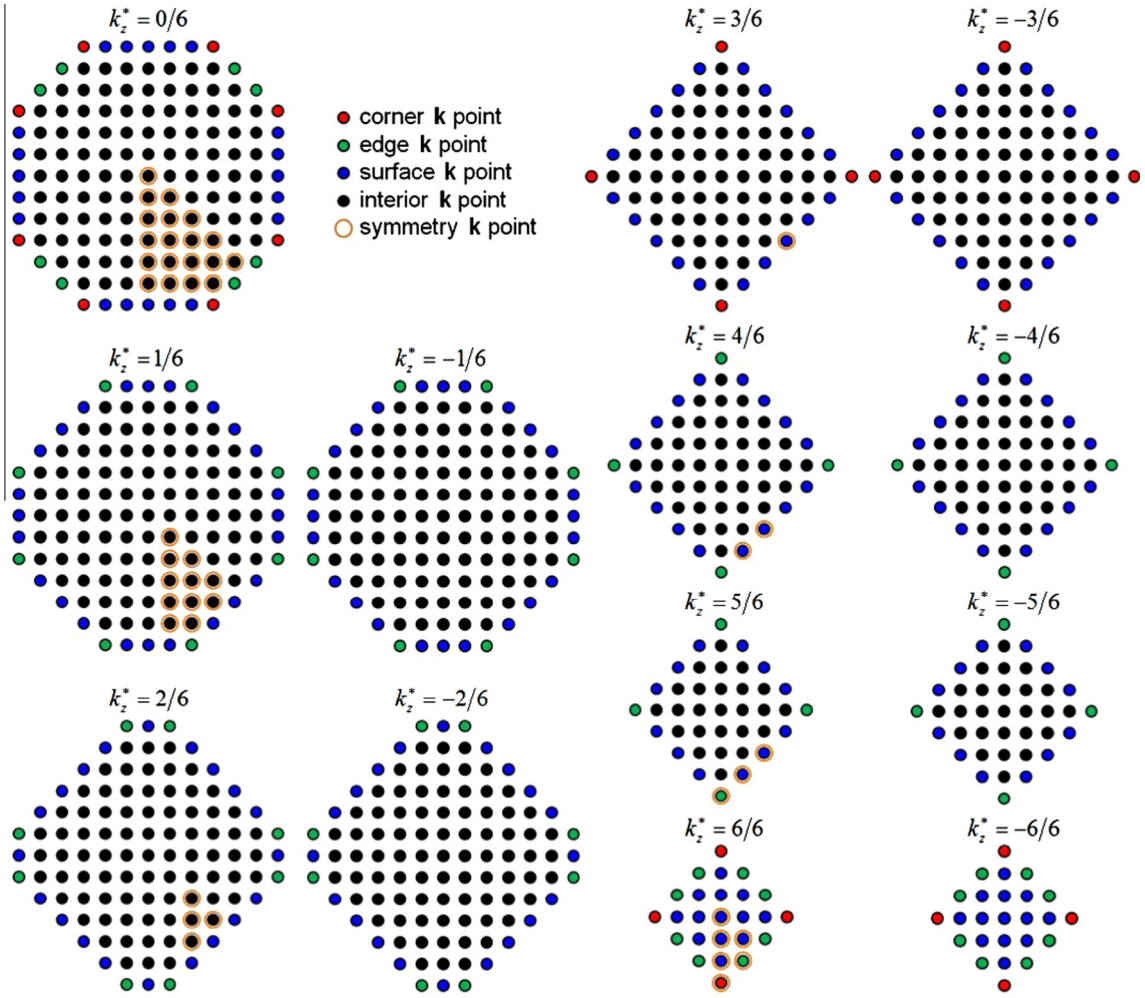

Fig. 2. The first Brillouin zone of an FCC crystal with $6 \times 6 \times 6$ conventional unit cells. The corner, edge, surface, and interior **k** points are filled in red, green, blue, and black, respectively. There are in total 864 non-degenerate **k** points. The 46 distinct **k** points based on symmetry considerations are enclosed by orange circles. Notice that k_z^* represents the z coordinates [with respect to $(\hat{\mathbf{x}}, \hat{\mathbf{y}}, \hat{\mathbf{z}})$] of the **k** points normalized with $\frac{2\pi}{a}$. (For interpretation of the references to color in this figure legend, the reader is referred to the web version of this article.)

edge **k** points exclude the corner **k** points, and the surface **k** points exclude the corner and edge **k** points. While the interior **k** points completely belong to the first Brillouin zone, the surface, edge, and corner **k** points are shared among 2, 3, and 4 neighboring first Brillouin zones, respectively. In Fig. 2, the corner, edge, surface, and interior **k** points are filled in red, green, blue, and black respectively to facilitate easy identification. By counting the number of interior, surface, edge, and corner **k** points and considering the associated sharing features, we can check whether or not the first Brillouin zone is correctly discretized.

To illustrate the idea of reducing the number of **k** points by symmetry considerations, we enclosed the symmetry **k** points with orange circles, as shown in Fig. 2. Since the **k** point layers all have reflection symmetry with respect to $k_x = 0$, $k_y = 0$, and $|k_x| = |k_y|$, we consider only 1/8 of the domain in each layer. Furthermore, the first Brillouin zone is symmetric with respect to $k_z = 0$, so the symmetry **k** points could be limited to the layers with nonnegative k_z^* values. In this work, we find it appropriate to indicate the interior symmetry **k** points in the layers with $k_z^* = 0/6$–$2/6$ and the surface, edge, and corner symmetry **k** points in the layers with $k_z^* = 3/6$–$6/6$. For the FCC crystal with $6 \times 6 \times 6$ conventional unit cells, there are in total 46 distinct symmetry **k** points. Table 1 shows the coordinates of the 46 symmetry **k** points and the number of equivalent **k** points associated with each of them. This number varies among 1, 3, 4, 6, 12, 24, and 48.

To ensure consistency, the sum of the $N_{\mathbf{k}_i,\mathrm{sym}}$ values must equal $4N_{\mathrm{cell}}^3$, which is 864 in the present case. This provides a way to check whether or not the symmetry **k** points are correctly determined. It should be noted that the above characteristics of the symmetry **k** points also exist in FCC crystals of other sizes and that the coordinates and the number of the corresponding symmetry **k** points could be determined in a similar way.

In addition to the consideration of symmetry from the geometrical point of view, we also examine the discretization of the first Brillouin zone of FCC crystals and the symmetry **k** points from an algebraic point of view. We find that for an FCC crystal with $N_{\mathrm{cell}} \times N_{\mathrm{cell}} \times N_{\mathrm{cell}}$ unit cells, the number of corner, edge, and surface **k** points are 6, $(6N_{\mathrm{cell}} - 12)$, and $(\frac{9}{2}N_{\mathrm{cell}}^2 - 9N_{\mathrm{cell}} + 7)$, respectively. Since the total number of **k** points is $4N_{\mathrm{cell}}^3$, the number of interior **k** points is found to be $(4N_{\mathrm{cell}}^3 - \frac{9}{2}N_{\mathrm{cell}}^2 + 3N_{\mathrm{cell}} - 1)$. To determine the coordinates of the symmetry **k** points, we consider a general expression of the **k** points as $\left(k_x^*, k_y^*, k_z^*\right)$, where k_x^*, k_y^*, and k_z^* represent the normalized **k** point coordinates and could

Table 1
Summary of the symmetry **k** points in the first Brillouin zone of an FCC crystal with $6 \times 6 \times 6$ conventional unit cells. The first column shows the indices of the **k** points. The second column shows the coordinates of the **k** points, which are with respect to the basis vector set $(\hat{\mathbf{x}}, \hat{\mathbf{y}}, \hat{\mathbf{z}})$ and normalized by $\frac{2\pi}{a}$. The third column shows the number ($N_{\mathbf{k}_i,\text{sym}}$) of **k** points that are equivalent to $\mathbf{k}_i$.

Index	$\mathbf{k}_i$ coordinates	$N_{\mathbf{k}_i,\text{sym}}$	Index	k_i coordinates	$N_{\mathbf{k}_i,\text{sym}}$	Index	k_i coordinates	$N_{\mathbf{k}_i,\text{sym}}$
1	(0.0000, 0.0000, 0.0000)	1	17	(0.6667, 0.5000, 0.0000)	24	33	(0.6667, 0.3333, 0.3333)	24
2	(0.1667, 0.0000, 0.0000)	6	18	(0.8333, 0.5000, 0.0000)	24	34	(0.5000, 0.5000, 0.3333)	24
3	(0.3333, 0.0000, 0.0000)	6	19	(0.6667, 0.6667, 0.0000)	12	35	(0.5000, 0.5000, 0.5000)	4
4	(0.5000, 0.0000, 0.0000)	6	20	(0.1667, 0.1667, 0.1667)	8	36	(0.6667, 0.1667, 0.6667)	12
5	(0.6667, 0.0000, 0.0000)	6	21	(0.3333, 0.1667, 0.1667)	24	37	(0.5000, 0.3333, 0.6667)	24
6	(0.8333, 0.0000, 0.0000)	6	22	(0.5000, 0.1667, 0.1667)	24	38	(0.6667, 0.0000, 0.8333)	8
7	(0.1667, 0.1667, 0.0000)	12	23	(0.6667, 0.1667, 0.1667)	24	39	(0.5000, 0.1667, 0.8333)	24
8	(0.3333, 0.1667, 0.0000)	24	24	(0.8333, 0.1667, 0.1667)	24	40	(0.3333, 0.3333, 0.8333)	12
9	(0.5000, 0.1667, 0.0000)	24	25	(0.3333, 0.3333, 0.1667)	24	41	(0.0000, 0.0000, 1.0000)	3
10	(0.6667, 0.1667, 0.0000)	24	26	(0.5000, 0.3333, 0.1667)	48	42	(0.1667, 0.0000, 1.0000)	12
11	(0.8333, 0.1667, 0.0000)	24	27	(0.6667, 0.3333, 0.1667)	48	43	(0.3333, 0.0000, 1.0000)	12
12	(0.3333, 0.3333, 0.0000)	12	28	(0.8333, 0.3333, 0.1667)	48	44	(0.5000, 0.0000, 1.0000)	6
13	(0.5000, 0.3333, 0.0000)	24	29	(0.5000, 0.5000, 0.1667)	24	45	(0.1667, 0.1667, 1.0000)	12
14	(0.6667, 0.3333, 0.0000)	24	30	(0.6667, 0.5000, 0.1667)	48	46	(0.3333, 0.1667, 1.0000)	16
15	(0.8333, 0.3333, 0.0000)	24	31	(0.3333, 0.3333, 0.3333)	8			
16	(0.5000, 0.5000, 0.0000)	12	32	(0.5000, 0.3333, 0.3333)	24			

have values from the set $\left\{\frac{0}{N_{\text{cell}}}, \pm\frac{1}{N_{\text{cell}}}, \pm\frac{2}{N_{\text{cell}}}, \ldots, \pm\frac{N_{\text{cell}}-1}{N_{\text{cell}}}, \frac{N_{\text{cell}}}{N_{\text{cell}}}\right\}$. The coordinates of the possible **k** points $\left(k_x^*, k_y^*, k_z^*\right)$ could be determined by imposing the following condition: $k_x^* + k_y^* + k_z^* \leqslant \frac{3}{2}$, and the **k** points could be categorized into seven mutually exclusive sets, as follows:

$$(1)\ S_{k,1} = \left\{\left(k_\alpha^*,\ k_\beta^*,\ k_\gamma^*\right) | k_\alpha^* k_\beta^* k_z^* \neq 0,\ k_\alpha^* = k_\beta^* = k_\gamma^*\right\};$$
$$(2)\ S_{k,2} = \left\{\left(k_\alpha^*,\ k_\beta^*,\ k_\gamma^*\right) | k_\alpha^* k_\beta^* k_\gamma^* \neq 0,\ k_\alpha^* = k_\beta^* \neq k_\gamma^*\right\};$$
$$(3)\ S_{k,3} = \left\{\left(k_\alpha^*,\ k_\beta^*,\ k_\gamma^*\right) | k_\alpha^* k_\beta^* k_\gamma^* \neq 0,\ k_\alpha^* \neq k_\beta^* \neq k_\gamma^*\right\};$$
$$(4)\ S_{k,4} = \left\{\left(k_\alpha^*,\ k_\beta^*,\ k_\gamma^*\right) | k_\alpha^* = 0,\ k_\beta^* = k_\gamma^* \neq 0\right\};$$
$$(5)\ S_{k,5} = \left\{\left(k_\alpha^*,\ k_\beta^*,\ k_\gamma^*\right) | k_\alpha^* = 0,\ k_\beta^* \neq k_\gamma^* \neq 0\right\};$$
$$(6)\ S_{k,6} = \left\{\left(k_\alpha^*,\ k_\beta^*,\ k_\gamma^*\right) | k_\alpha^* = 0,\ k_\beta^* = 0,\ k_\gamma^* \neq 0\right\};$$
$$(7)\ S_{k,7} = \left\{\left(k_\alpha^*,\ k_\beta^*,\ k_\gamma^*\right) | k_\alpha^* = 0,\ k_\beta^* = 0,\ k_\gamma^* = 0\right\}.$$

Here, α, β, and γ is a possible combination of x, y, and z. The symmetry **k** points could be determined by examining the coordinates of the **k** points in the sets $S_{k,i}$ $(i = 1, 2, \ldots, 7)$. The number of equivalent **k** points associated with each symmetry **k** point could then be determined by considering permutations and combinations. It should be noted that when counting the number of equivalent **k** points associated with a symmetry **k** point, we must take into account the distinct sharing features of the interior, surface, edge, and corner **k** points. This means the possible number of equivalent **k** points obtained from permutations and combinations for the interior, surface, edge, and corner symmetry **k** points should be corrected by multiplying a factor of 1, $\frac{1}{2}$, $\frac{1}{3}$, and $\frac{1}{4}$, respectively. As an example, the number of **k** points associated with an interior symmetry **k** point in $S_{k,3}$ is ${}_3\text{P}_3 \times 2^3 \times 1$ (=48), where the "${}_3\text{P}_3$" represents the permutations of k_α^*, k_β^*, and k_γ^*, the "2^3" accounts for the positive and negative values of k_α^*, k_β^*, and k_γ^*, and the "1" is the multiplication factor for interior **k** points. Similarly, the number of **k** points associated with an edge **k** point in $S_{k,5}$ is ${}_3\text{P}_3 \times 2^2 \times \frac{1}{3}$ (=8), where the "${}_3\text{P}_3$" represents the permutations of k_α^*, k_β^*, and k_γ^*, the "2^2" accounts for the positive and negative values of k_β^* and k_γ^*, and the "$\frac{1}{3}$" indicates the sharing of the edge **k** point among three neighboring first Brillouin zones. In the same manner, the number of equivalent **k** points associated with all the interior, surface, edge, and corner **k** points in the sets $S_{k,i}$ $(i = 1, 2, \ldots, 7)$ could be determined.

Using this analysis method, we have calculated the number of different types of equivalent **k** points in the first Brillouin zone of an FCC crystal with N_{cell} ranging from 2 to 20, as summarized in Table 2. Here we consider only even N_{cell} values for simplicity of discretizing the first Brillouin zone. It is seen that as N_{cell} increases, the number of corner **k** points remains six, but the number of edge, surface, and interior **k** points all increase. The rate of increase of the number of surface **k** points is higher than that of edge **k** points but lower than that of interior **k** points. This is consistent with the earlier analysis in this work, which has shown that $N_{\mathbf{k},\text{edge}} \sim O(N_{\text{cell}})$, $N_{\mathbf{k},\text{surface}} \sim O(N_{\text{cell}}^2)$, and $N_{\mathbf{k},\text{interior}} \sim O(N_{\text{cell}}^3)$. As N_{cell} increases from 2 to 20, the number of symmetry **k** points increases from 6 to 916. Previously, McGaughey [15] studied the first Brillouin zone of a solid argon crystal with $N_{\text{cell}} = 4$ and obtained 18 instead of 20 symmetry **k** points. The reason for the discrepancy is that McGaughey neglected the Γ point and combined the **k** point $(1.00, 0.25, 0.25)$ [equivalent to $(0.25, 0.25, 1.00)$ in our study] with the **k** point $(0.75, 0.75, 0.00)$ [equivalent to $(0.75, 0.00, 0.75)$ in our study].

To examine the extent to which the symmetry **k** points could reduce the total number of **k** points, we vary N_{cell} from 2 to 256 and calculate the percentage reduction of the total number of **k** points, which is defined as $\%\text{RED} = \frac{N_{\mathbf{k},\text{total}} - N_{\mathbf{k},\text{sym}}}{N_{\mathbf{k},\text{total}}} \times 100\%$. From the results in Fig. 3, we notice that as N_{cell} increases, the %RED increases and gradually approaches an upper limit. To estimate this upper limit, we consider a crystal with $N_{\text{cell}} \to \infty$, in which

Table 2
The number of different types of **k** points in the first Brillouin zone of an FCC crystal with $N_{\text{cell}} = 2$–20. The $N_{\mathbf{k},\text{corner}}$, $N_{\mathbf{k},\text{edge}}$, $N_{\mathbf{k},\text{surface}}$, $N_{\mathbf{k},\text{interior}}$, $N_{\mathbf{k},\text{total}}$, and $N_{\mathbf{k},\text{sym}}$ represent the number of corner, edge, surface, interior, total, and symmetry **k** points, respectively.

N_{cell}	$N_{\mathbf{k},\text{corner}}$	$N_{\mathbf{k},\text{edge}}$	$N_{\mathbf{k},\text{surface}}$	$N_{\mathbf{k},\text{interior}}$	$N_{\mathbf{k},\text{total}}$	$N_{\mathbf{k},\text{sym}}$
2	6	0	7	19	32	6
4	6	12	43	195	256	20
6	6	24	115	719	864	46
8	6	36	223	1783	2048	89
10	6	48	367	3579	4000	152
12	6	60	547	6299	6912	240
14	6	72	763	10,135	10,976	356
16	6	84	1015	15,279	16,384	505
18	6	96	1303	21,923	23,328	690
20	6	108	1627	30,259	32,000	916

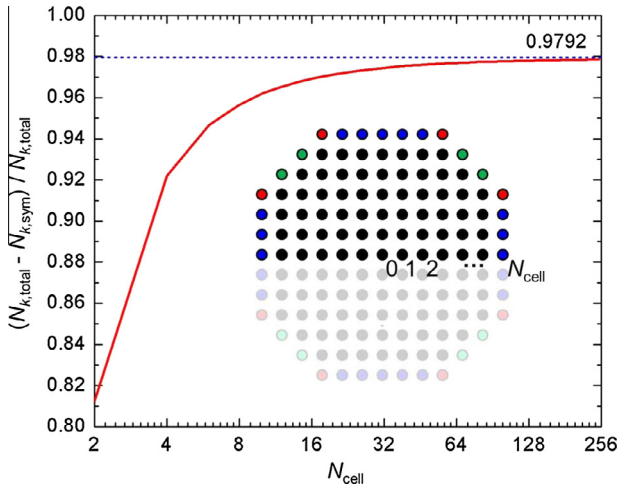

Fig. 3. Variation of the percentage reduction of the total number of **k** points by using the symmetry **k** points with respect to N_{cell}. The dashed line shows the upper limit ($\frac{48-1}{48} \approx 0.9792$) of the percentage reduction of the total number of **k** points. The inset shows the **k** point layer with $k_z^* = 0$ for an FCC crystal with $N_{\text{cell}} = 6$.

the number of corner, edge, and surface **k** points becomes so small compared with that of interior **k** points that only the interior **k** points need to be taken into account. Furthermore, the interior symmetry **k** points will predominantly have coordinates $\left(k_x^*, k_y^*, k_z^*\right)$ satisfying $k_x^* \neq k_y^* \neq k_z^* \neq 0$, and each of these **k** points is associated with 48 equivalent **k** points. Therefore, the upper limit of the %RED could be estimated as $\frac{48-1}{48} (\approx 0.9792)$. At $N_{\text{cell}} = 256$, the %RED reaches a value 0.9786, which differs from the upper limit by merely 0.06%. Therefore, using symmetry **k** points is an effective way of reducing the number of **k** points to be explicitly considered.

Since both our method and the irreducible first Brillouin zone method utilize the symmetry operations of the first Brillouin zone of FCC crystals, we provide a comparison between the two methods. The major difference between the two methods is that our method has a direct correspondence to the crystal structure and ensures the consistency of the number of degrees of freedom in the direct and reciprocal spaces, while the irreducible first Brillouin zone method is purely geometric and the **k** point grid could be chosen arbitrarily. For example, if a **k** point grid of size $6 \times 6 \times 6$ is used to sample the first Brillouin zone of an FCC crystal, the irreducible first Brillouin zone method reduces the number of **k** points from 216 to 20, and similar reductions exist for **k** point grid of other sizes. On the other hand, our method is actually not designed for this kind of **k** point reductions. Instead, if we consider an FCC crystal of a size $6 \times 6 \times 6$ conventional unit cells, our method reduces the number of **k** points from 864 to 46. In this sense, the two methods are not directly comparable, although they both utilize the symmetries of the first Brillouin zone of FCC crystals. One disadvantage of our method is its limited capabilities. In the current form, it can only deal with FCC crystals with a single basis atom and an even number of conventional unit cells in each coordinate direction. Further studies could be conducted to extend the capabilities of our method to handle FCC crystal systems of other geometrical features. However, our method has a significant advantage: it allows generation of the coordinates of the symmetry **k** points in the first Brillouin zone of FCC crystals in a systematic way and the generated **k** point coordinates could then be used in subsequent spectral analysis, which is particularly useful when the spectral analysis is done by using in-house codes. Regarding thermal conductivity calculations, both methods should give the same result in the convergent limit.

Another comment about our method is that it may not be applicable to calculations related to phonon scattering processes, which require satisfactions of crystal momentum and phonon energy conservations. The reason is that while the energies of the phonons in a particular branch and at equivalent **k** points could be assumed to be the same, the crystal momentums, which are vectors, depend on the coordinates of the **k** points. As a result, the entire first Brillouin zone has to be sampled in studies related to phonon scattering processes (*e.g.*, anharmonic lattice dynamics calculations).

We move on to discuss how the results corresponding to the entire first Brillouin zone could be recovered from the results obtained with the symmetry **k** points. As an example, we consider lattice thermal conductivity. According to the Boltzmann transport equation under the relaxation time approximation in combination with the Fourier's law, the lattice thermal conductivity of a crystal in the x direction can be calculated as [36]

$$\kappa_x = \sum_{\mathbf{k}} \sum_{\nu} c_{\text{ph}}(\mathbf{k}, \nu) v_{g,x}^2(\mathbf{k}, \nu) \tau(\mathbf{k}, \nu), \tag{1}$$

where $c_{\text{ph}}(\mathbf{k}, \nu)$ is the per mode phonon specific heat, $v_{g,x}(\mathbf{k}, \nu)$ is the x component of the phonon group velocity, and $\tau(\mathbf{k}, \nu)$ is the phonon relaxation time, respectively, of the phonon mode $(\mathbf{k}, \nu)$, which has a wavevector **k** and lies in the νth phonon branch. By using the symmetry **k** points, we propose the following formula

$$\kappa_{x,\text{sym}} = \sum_{\mathbf{k}_{\text{sym}}} \sum_{\nu} c_{\text{ph,eq}}(\mathbf{k}_{\text{sym}}, \nu) v_{g,x}^2(\mathbf{k}_{\text{sym}}, \nu) \tau(\mathbf{k}_{\mathbf{sym}}, \nu), \tag{2}$$

where $\mathbf{k}_{\text{sym}}$ represents the symmetry **k** points and $c_{\text{ph,eq}}(\mathbf{k}_{\text{sym}}, \nu) = N(\mathbf{k}_{\text{sym}}) c_{\text{ph}}(\mathbf{k}_{\text{sym}}, \nu)$ is the equivalent phonon specific heat. Here $N(\mathbf{k}_{\text{sym}})$ is the number of equivalent **k** points associated with the corresponding symmetry **k** point. The essential assumption in Eq. (2) is that the phonon modes at the equivalent **k** points have the same phonon properties (*i.e.*, c_{ph}, $v_{g,x}$, and τ). To validate this formula, we show a case study on solid argon in the following section.

4. A case study on solid argon

In this section, we report results on the thermal conductivity of solid argon from EMD simulations and SED analysis, which provide a validation to Eq. (2). We also report the phonon relaxation times in solid argon and the thermal conductivity accumulation profiles with respect to the phonon wavelength and MFP.

Using the `LAMMPS` package [37], we conducted EMD simulations to calculate the thermal conductivity of solid argon in the temperature range from 10 to 80 K. We considered a maximum temperature of 80 K because solid argon has a melting point of $T_{\text{m}} \approx 84$ K [38,39]. We observed from the atomic trajectories that even at 80 K the atoms vibrate around their equilibrium positions. In addition, it has been shown that the magnitude of atomic vibrations in solid argon at 80 K is less than 5% of the nearest atomic separation [15]. The interatomic interactions in solid argon are characterized with the Lennard-Jones potential [17] as

$$U = 4\epsilon \left[\left(\frac{\sigma}{r_{ij}} \right)^{12} - \left(\frac{\sigma}{r_{ij}} \right)^{6} \right], \tag{3}$$

where ϵ (=119.8k_{B}) is the potential well depth, σ (=3.405 Å) is the interatomic distance, at which the potential energy reaches zero, and r_{ij} is the separation between atoms i and j. The potential cutoff radius r_{cutoff} was set as 3.1σ, at which the potential energy is decreased to 1.0% of that at the equilibrium interatomic distance. Periodic boundary conditions were applied in the x, y, and z directions. The time step was set to be 4.0 fs, which is sufficient to resolve the highest-frequency phonon mode ($f_{\text{max}} \sim 2$ THz). In each simulation, the material system was first relaxed in an isothermal–

isobaric ensemble (NPT) for 0.4 ns to achieve a zero pressure and the prescribed temperature by using a Nosé–Hoover barostat and thermostat [40,41], respectively. After that, the material system was simulated in a microcanonical ensemble (NVE) for 4.0 ns for data production. We calculate the thermal conductivities by using the Green–Kubo (GK) formula as [42]

$$\kappa = \frac{V}{3k_B T^2}\int_0^{t_0} \mathbf{J}(0)\cdot\mathbf{J}(t)\mathrm{d}t, \tag{4}$$

where V is the volume of the material system, k_B is the Boltzmann constant, T is temperature, t_0 is the correlation length of the heat current autocorrelation function (HCACF) $\mathbf{J}$, and the factor "$\frac{1}{3}$" indicates the isotropic assumption of the thermal conductivities. For the pair interactions considered in this study, the heat current vector is computed as [19,20]

$$\mathbf{J} = \frac{1}{V}\left[\sum_i \epsilon_i \mathbf{v}_i + \frac{1}{2}\sum_{i\neq j}(\mathbf{F}_{ij}\cdot\mathbf{v}_i)\mathbf{r}_{ij}\right], \tag{5}$$

where ϵ_i and $\mathbf{v}_i$ are the site energy and velocity of the atom i respectively, and $\mathbf{F}_{ij}$ is the interatomic force between the atoms i and j. Based on some trial simulations, we set the correlation lengths of the HCACF to be 80,000, 40,000, and 20,000 time steps for the simulations at temperatures of 10, 20, and 30 K, respectively. At temperatures above 30 K, the correlation lengths were set as 10,000 time steps. To reduce statistical errors, we ran each simulation for 10 times with different initial velocity distributions and report the average results from the 10 repetitions.

We also conducted SED analysis to extract the spectral phonon properties and thereafter calculate the thermal conductivity by using Eq. (2). Since the detailed formulations of the SED analysis method are available in the literature [22,28,36,43], here we provide a brief summary. In SED analysis, the atomic velocities from EMD simulations are used as inputs. By calculating the squared magnitude of the Fourier transformed velocities, an SED function can be constructed for each $\mathbf{k}$ point. By fitting the phonon spectral peaks in the SED functions using Lorentzian functions, the spectral phonon relaxation times can be obtained as

$$\tau(\mathbf{k},\nu) = \frac{1}{2\gamma(\mathbf{k},\nu)}, \tag{6}$$

where γ is the half-width at half-maximum of a Lorentzian peak. We observed that even at 80 K the SED peaks could still be fit to Lorentzian peaks reasonably well. In the SED analysis at different temperatures, we considered the quasi-harmonic approximation and used temperature-dependent lattice constants. From a size effect study, we found that the thermal conductivity of argon converges at a size of $6\times6\times6$ conventional unit cells at $T = 10, 40,$ and 80 K (see Fig. 4). So this size was selected for the EMD simulations and the SED analysis. We notice that both GK-MD simulations and SED analysis have size effects [44,27]. Ideally a series of simulations should be conducted on material systems of different sizes and the results extrapolated to correspond to an infinitely large system. In this study, we decided not to adopt this approach for the purpose of simplicity and also because this study is mainly focused on the $\mathbf{k}$ point reduction in the first Brillouin zone of FCC crystals. Another reason was to keep the number of degrees of freedom in the MD simulations and SED analysis to be the same so that the results are directly comparable. Further studies could be performed to provide a detailed examination of the size effects of GK-MD simulations and SED analysis by using the method developed in this work and the extrapolation approach. To resolve the $\mathbf{k}$ points in the first Brillouin zone, we considered the symmetry $\mathbf{k}$ points, which reduces the total number of $\mathbf{k}$ points from 864 to 46 (see Table 2) and thus greatly reduces the computational cost.

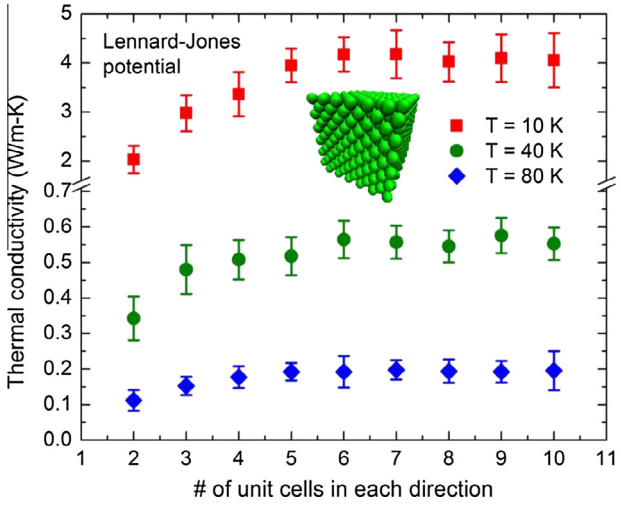

Fig. 4. Size effect of the thermal conductivities of solid argon at 10, 40, and 80 K, respectively. The thermal conductivities are calculated from the EMD simulations with the Lennard-Jones potential.

After obtaining the spectral phonon frequencies and relaxation times, we calculated the thermal conductivity according to Eq. (2). Because argon has a Debye temperature of about 85 K [38,45] and MD simulations are reasonably accurate at temperatures down to 1/10 of the Debye temperature [46] which is lower than the lowest temperature (10 K) considered in this study, we neglected quantum effects and calculated the per mode phonon specific heat as $c_{\mathrm{ph}} = \frac{k_B}{V}$, where V is the crystal volume. To obtain the total crystal specific heat, we need to multiply c_{ph} by a factor of 2592 ($=6\times6\times6\times4\times3$). Because temperature has a small effect on phonon dispersions [47], we calculated the phonon group velocities by using the phonon dispersions from `GULP` [29] which corresponds to 0 K. We also made the isotropic assumption and considered only the phonon dispersions in the Γ–X direction. To account for the spatial distribution of the $\mathbf{k}$ points, we computed the group velocities as $v_{g,x} = \mathbf{v}_g\cdot\mathbf{k}$, where $\mathbf{v}_g$ $(=\frac{\partial\omega}{\partial\mathbf{k}})$ was calculated based on the phonon dispersions from `GULP` [29] and with a central difference scheme.

4.1. Thermal conductivity

In this subsection, we present the thermal conductivities of solid argon calculated with the Lennard-Jones potential in the temperature range from 10 to 80 K. The thermal conductivities were calculated using either EMD simulations in combination with the Green–Kubo formula (Eq. (4)) or SED analysis.

Since the lattice thermal conductivity of a crystal depends on its size [48], we examined the size dependence of the thermal conductivity of solid argon using EMD simulations. Fig. 4 shows the thermal conductivity of solid argon at temperatures 10, 40, and 80 K respectively as a function of the crystal size, which is measured as the number of conventional unit cells in each direction. Notice that all the crystals considered in this study are cubic, as seen in the inset of Fig. 4. At all the three temperatures, the thermal conductivity first increases with the increasing crystal size and then gradually approaches a converged value. As temperature increases, the crystal size at which the thermal conductivity reaches convergence decreases. It is seen that the thermal conductivity of solid argon converges at a crystal size of $6\times6\times6$ conventional unit cells at 10 K and $4\times4\times4$ conventional unit cells at 80 K. Although a crystal size of $4\times4\times4$ conventional unit cells was adopted in previous studies [15], we recommend that future studies on solid

argon use material systems no smaller than $6 \times 6 \times 6$ conventional unit cells, especially when the thermal conductivities and spectral phonon properties at low temperatures are of interest. In this work, the following calculations on the thermal conductivities and spectral phonon relaxation times of solid argon all correspond to a crystal with a size of $6 \times 6 \times 6$ conventional unit cells.

In Fig. 5, we show the thermal conductivities calculated from the EMD simulations and those from the SED analysis, which are compared with the experimental values by Touloukian [39]. The inset of Fig. 5 shows the convergence of the normalized HCACFs from an EMD simulation at 40 K. In calculating thermal conductivities using EMD simulations with the Green–Kubo formula, it is crucial to ensure that the HCACF is converged. It is well known that HCACF has a longer correlation length at a lower temperature. Based on some trial simulations, we found that correlation lengths of 0.32, 0.16, 0.08, and 0.04 ns are sufficient for simulations at temperatures 10, 20, 30, and $\geqslant$40 K, respectively. In Fig. 5, we observe that the calculated thermal conductivities agree well with the experimental values, although the values at temperatures higher than 50 K are slightly lower than the corresponding experiment ones. Similar results have been reported in previous studies [19,49,22]. As temperature increases from 10 to 80 K, the thermal conductivity decreases from 3.7 to 0.3 W/m K. The error bars, calculated as the standard deviations of the values from the repetitive simulations, also decrease with increasing temperature. The thermal conductivities obtained from the SED analysis are in good agreement with the experimental data at temperatures higher than 20 K. The slightly lower value at 10 K could be attributed to the quantum effects in the phonon specific heats. This overall good agreement provides a justification to the applicability of Eq. (2), which uses phonon properties at the symmetry **k** points instead of those at all the **k** points in the first Brillouin zone, to calculate lattice thermal conductivities.

4.2. Phonon relaxation time

In Fig. 6, we show the spectral phonon relaxation times of solid argon at temperatures 20, 40, 60, and 80 K, respectively. As temperature increases, the phonon relaxation times decrease as a result of the increased phonon scattering rates. At a prescribed temperature, the phonon relaxation times decrease with increasing

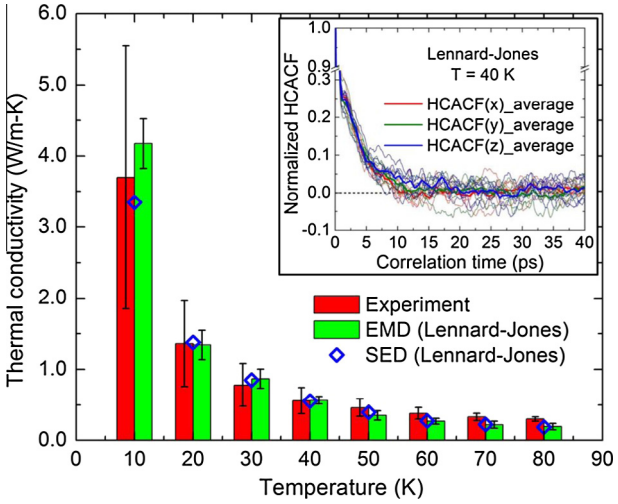

Fig. 5. Comparison of the experimental and numerical thermal conductivities of solid argon in the temperature range from 10 to 80 K. The numerical values include those from the EMD simulations and those from the SED analysis. The experimental data are by Touloukian [39]. The inset shows the decay of the normalized heat current autocorrelation function (HCACF) in the EMD simulations at 40 K.

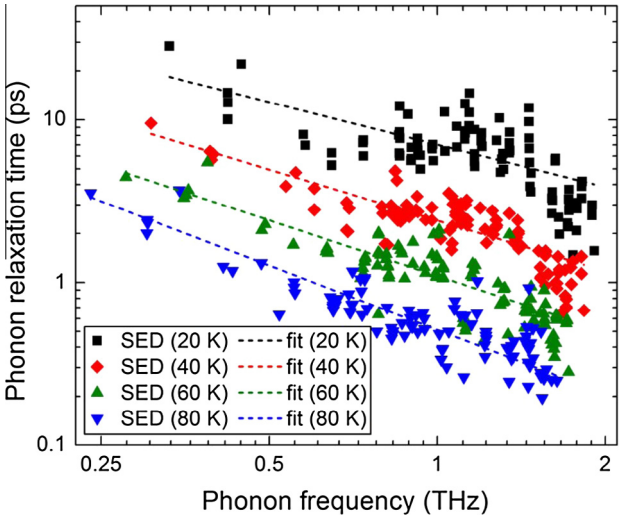

Fig. 6. Spectral phonon relaxation times of solid argon at temperatures 20, 40, 60, and 80 K. The dashed lines show the power fits of the phonon relaxation times with the phonon frequency.

phonon frequency, which could be attributed to the more scattering events associated with the high frequency phonons. As a comparison, the predicted spectral phonon relaxation times are in good agreement with the previous predictions [15,23,25]. It should be noted that we made no differentiation on the different phonon branches in this study.

The dashed lines in Fig. 6 show the fits of the relaxation times according to the formula $\tau = a\omega^b$, where τ is phonon relaxation time (and τ^{-1} is phonon scattering rate), ω is phonon frequency, and a and b are fitting parameters. Since the horizontal and vertical axes in Fig. 6 are plotted in logarithmic scales, the power fits appear linear. We notice that the slope of the fitted lines increases (becoming more negative) with increasing temperature. The detailed fitting parameters are summarized in Table 3. It is seen that as temperature increases from 20 to 80 K, the slope of the fitted lines decreases from -0.87 to -1.31. Previously, an analytical model for phonon scattering rates (or phonon relaxation times) has been proposed of the form [46,50]

$$\tau^{-1} = B\omega^n T^m, \tag{7}$$

where B, n, and m are fitting parameters. Although this model is relatively rudimental, it could be used to capture the basic features of the phonon relaxation time dependence on phonon frequency and temperature for both normal and umklapp scattering processes over a wide range of phonon frequencies and temperatures [50]. Depending on the temperature range and the scattering processes, usually n has a value of 1 or 2, and m has a value of 1, 3, or 4. In Table 3, we see that the index (b) of the phonon frequency decreases with increasing temperature, indicating a stronger frequency dependence of the phonon relaxation times at a higher temperature. Since the indices $(-b)$ are all around one, we conclude that the phonon relaxation times from the SED analysis are consistent with the predictions of the analytical model. The deviations of the indices from unity could be caused by thermal expansion effects [51,20].

Table 3
Fitting parameters of the power fits of the phonon relaxation times shown in Fig. 6.

T (K)	20	40	60	80
a	7.05	2.41	1.10	0.51
b	−0.87	−1.04	−1.13	−1.31

With the spectral phonon relaxation times, we computed the average phonon relaxation times as

$$\tau_{ave}(T) = \frac{\sum_{\mathbf{k}}\sum_{v} c_{ph,eq}(\mathbf{k},v,T)\, v_{g,x}^2(\mathbf{k},v,T)\,\tau(\mathbf{k},v,T)}{\sum_{k}\sum_{v} c_{ph,eq}(\mathbf{k},v,T)\, v_{g,x}^2(\mathbf{k},v,T)}. \quad (8)$$

The results, together with the phonon specific heats, are shown in Fig. 7. As temperature increases from 10 to 80 K, the average phonon relaxation time decreases from 12.1 to 0.5 ps due to the more phonon scattering events at higher temperatures, and the per mode phonon specific heat decreases from 432.7 to 384.5 J/m^3 K due to thermal expansion of the crystal structure. A power fit of the average phonon relaxation times shows that the average phonon relaxation times decrease with temperature according to $T^{-1.28}$. Considering the relatively weak temperature dependence of the phonon specific heats and group velocities, we conclude that the decreasing thermal conductivity of solid argon with increasing temperature, as seen in Fig. 5, is mainly caused by the reduction in the phonon relaxation times.

4.3. Thermal conductivity accumulation

Thermal conductivity accumulation with phonon wavelength and MFP provides information on the important length scales of thermal transport in materials. In Fig. 8, we show the thermal conductivity accumulation of solid argon at 40 K with respect to phonon wavelength and MFP, which are calculated based on the spectral phonon properties from the SED analysis as

$$k_{accum}(\lambda^*) = \sum_{\mathbf{k}}\sum_{v} c_{ph,eq}(\mathbf{k},v,\lambda)\, v_{g,x}^2(\mathbf{k},v,\lambda) \times \tau(\mathbf{k},v,\lambda) \quad \text{for } 0 \leqslant \lambda \leqslant \lambda^*, \quad (9)$$

where λ^* represents the cutoff phonon wavelength or MFP. The converged thermal conductivity is found to be 0.61 W/m K, and the experimental value (0.56 ± 0.18 W/m K) [39]. In Fig. 8, it is seen that 80% of the thermal conductivity of solid argon at 40 K is contributed by phonons with wavelengths less than 0.92 nm and by phonons with MFPs less than 3.7 nm, respectively. These relatively small values are due to the small phonon relaxation times which are originated from the weak van der Waals forces in solid argon. The thermal conductivity accumulation profiles could be used for analyzing or designing the thermal conductivity of solid argon material systems. For example, if a solid argon material system has a dimension of about 3 nm in a particular direction, we would expect the thermal conductivity in that direction to be about 55% of the bulk value. On the other hand, if a thermal conductivity of about 90% of the bulk value is desired, we could design a solid argon material system with a dimension of about 4.2 nm in the direction of interest.

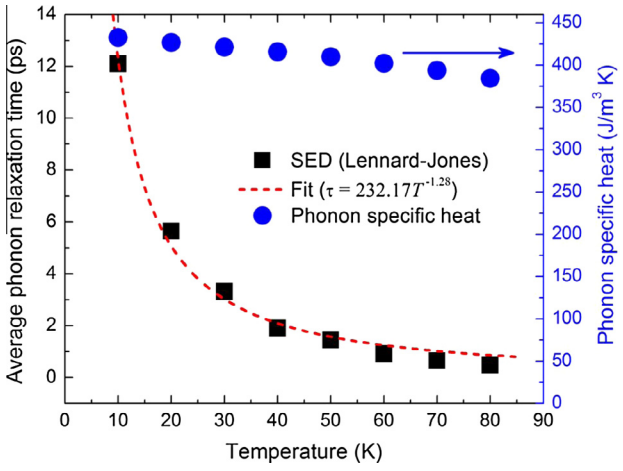

Fig. 7. Variation of the average phonon relaxation time and phonon specific heat of solid argon with temperature. The dashed line shows a power fit of the average phonon relaxation times with temperature.

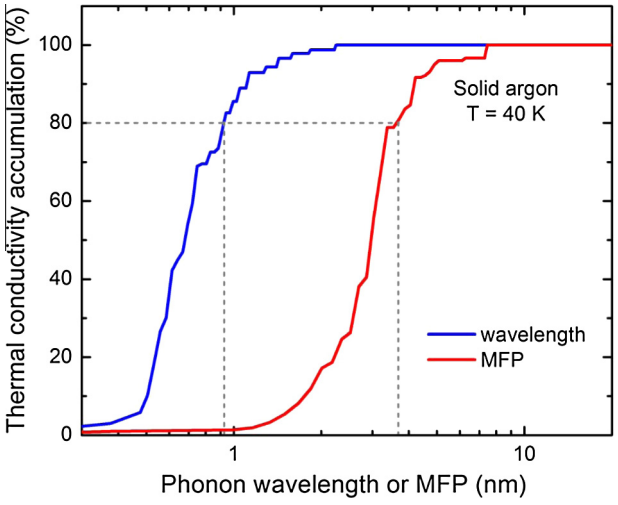

Fig. 8. Thermal conductivity accumulation of solid argon at 40 K with phonon wavelength and MFP. The dashed lines indicate an eighty percent accumulation and the corresponding phonon wavelength and MFP.

5. Conclusions

In this work, we have examined the geometry and discretization of the first Brillouin zone of FCC crystals. The coordinates of the high symmetry **k** points are reported with respect to the basis vector sets $(\hat{\mathbf{x}}, \hat{\mathbf{y}}, \hat{\mathbf{z}})$ and $(\mathbf{b}_1, \mathbf{b}_2, \mathbf{b}_3)$. We have proposed a way of reducing the total number **k** points by using the symmetry **k** points. A systematic procedure is presented to determine the coordinates and degeneracy of the symmetry **k** points. By using the symmetry **k** points, the number of **k** points that need to be explicitly resolved could be reduced by as much as 97.92%. We have also proposed a formula for calculating the lattice thermal conductivity of FCC crystals by considering only the symmetry **k** points. The formula is validated by calculating the thermal conductivity of solid argon in the temperature range from 10 to 80 K using the phonon spectral energy density (SED) method. As temperature increases from 10 to 80 K, the thermal conductivity decreases from about 3.7 to 0.3 W/m K, which is mainly due to the reduction in the phonon relaxation times. We also find that 80% of the thermal conductivity of solid argon at 40 K is contributed by phonons with wavelengths less than 0.92 nm and by phonons with MFPs less than 3.7 nm, respectively. This work is potentially useful for other spectral analysis on the electronic, thermal, and optical properties of FCC crystals.

Acknowledgements

The financial support from the National Science Foundation (Award No. 1150948) and Purdue University is gratefully appreciated.

References

[1] C. Kittel, Introduction to Solid State Physics, Wiley, New York City, 2005.
[2] R.E. Hummel, Electronic Properties of Materials, Springer, Berlin, 1992.
[3] H.J.F. Jansen, A.J. Freeman, Phys. Rev. B 30 (1984) 561.
[4] W. Setyawan, S. Curtarolo, Comput. Mater. Sci. 49 (2010) 299.

[5] T.H. Hsieh, H. Lin, J. Liu, W. Duan, A. Bansil, L. Fu, Nat. Commun. 3 (2012) 982.
[6] F. Cleri, V. Rosato, Phys. Rev. B 48 (1993) 22.
[7] A.J.H. McGaughey, M. Kaviany, Phys. Rev. B 69 (2009) 094303.
[8] N. de Koker, Phys. Rev. Lett. 103 (2009) 125902.
[9] A. Chernatynskiy, S.R. Phillpot, Phys. Rev. B 82 (2010) 134301.
[10] K. Sakoda, Optical Properties of Photonic Crystals, Springer, New York, 2005.
[11] W.Y. Ching, M.Z. Huang, Y.N. Xu, W.G. Harter, F.T. Chan, Phys. Rev. Lett. 67 (1991) 2045.
[12] V.N. Bogomolov et al., Phys. Rev. E 55 (1997) 7619.
[13] J.F. Liu, H.X. Jiang, C.J. Jin, X.H. Wang, Z.S. Gan, B.H. Jia, M. Gu, Phys. Rev. A 85 (2012) 015802.
[14] G. Gilat, L.J. Raubenheimer, Phys. Rev. 144 (1966) 390.
[15] A.J.H. McGaughey, Ph.D. Thesis, University of Michigan, 2004.
[16] O.G. Peterson, D.N. Batchelder, R.O. Simmons, Phys. Rev. 150 (1966) 703.
[17] M.P. Allen, D.J. Tildesley, Computer Simulation of Liquids, Clarendon, Oxford, 1987.
[18] A.J.H. McGaughey, M. Kaviany, Int. J. Heat Mass Transfer 47 (8) (2004) 1783.
[19] K.V. Tretiakov, S. Scandolo, J. Chem. Phys. 120 (2004) 3765.
[20] Y. Chen, J.R. Lukes, D. Li, J. Yang, Y. Wu, J. Chem. Phys. 120 (2004) 3841.
[21] Z.X. Huang, Z.A. Tang, Physica B 373 (2006) 291.
[22] J.E. Turney, A.J.H. McGaughey, C.H. Amon, Phys. Rev. B 79 (2009) 224305.
[23] H. Bao, Acta Phys. Sin. 62 (2013) 186302.
[24] J.E. Turney, Ph.D. Thesis, Carnegie Mellon University, 2009.
[25] T. Feng, Master's Thesis, Purdue University, 2013.
[26] T. Feng, B. Qiu, X. Ruan, J. Appl. Phys. 117 (2015) 195102.
[27] J.M. Larkin, J.E. Turney, A.D. Massicotte, C.H. Amon, A.J.H. McGaughey, J. Comput. Theor. Nanosci. 11 (2014) 249.
[28] Z. Wang, T. Feng, X. Ruan, J. Appl. Phys. 117 (2015) 084317.
[29] J.D. Gale, A.L. Rohl, Mol. Simul. 29 (2003) 291.
[30] X. Gonze et al., Zeit. Kristallogr. 220 (2005) 558.
[31] X. Gonze et al., Comput. Phys. Commun. 180 (2009) 2582.
[32] P. Giannozzi et al., J. Phys.: Condens. Matter. 21 (2009) 395502.
[33] G. Kresse, J. Hafner, Phys. Rev. B 47 (1993) 558.
[34] G. Kresse, J. Hafner, Comput. Mater. Sci. 6 (1996) 15.
[35] G. Kresse, J. Furthmüller, Phys. Rev. B 54 (1996) 11169.
[36] J.A. Thomas, J.E. Turney, R.M. Lutzi, C.H. Amon, A.J.H. McGaughey, Phys. Rev. B 81 (2010) 081411.
[37] S. Plimpton, J. Comp. Phys. 117 (1995) 1.
[38] D.K. Christen, G.L. Pollack, Phys. Rev. B 12 (1975) 3380.
[39] Y. Touloukian, Thermophysical Properties of Matter, vol. 3, Plenum, New York, 1970.
[40] S. Nosé, J. Chem. Phys. 81 (1984) 511.
[41] W.G. Hoover, Phys. Rev. A 31 (1985) 1695.
[42] D.A. McQuarrie, Statistical Mechanics, University Science Books, Sausalito, 2000.
[43] A.S. Henry, G. Chen, J. Comput. Theor. Nanosci. 5 (2008) 1.
[44] K. Esfarjani, G. Chen, H.T. Stokes, Phys. Rev. B 84 (2011) 085204.
[45] N.W. Ashcroft, N.D. Mermin, Solid State Physics, Saunders College Publishing, For Worth, 1976.
[46] M. Kaviany, Heat Transfer Physics, Cambridge University Press, New York, 2014.
[47] A.J.H. McGaughey, M. Kaviany, Phys. Rev. B 69 (2004) 094303.
[48] P.K. Schelling, S.R. Phillpot, P. Keblinski, Phys. Rev. B 65 (2002) 144306.
[49] A.J.H. McGaughey, M. Kaviany, Int. J. Heat Mass Transfer 47 (2004) 1783.
[50] T. Feng, X. Ruan, J. Nanomater. 2014 (2014) 206370.
[51] F. Clayton, D.N. Batchelder, J. Phys. C: Solid State Phys. 6 (1973) 1213.